JOURNAL OF GEOPHYSICAL RESEARCH, VOL. 112, F02034, doi:10.1029/2006JF000574, 2007

Mechanics of river mouth bar formation: Implications for the morphodynamics of delta distributary networks

D. A. Edmonds[1] and R. L. Slingerland[1]

Received 10 May 2006; revised 20 October 2006; accepted 3 January 2007; published 20 June 2007.

[1] In this paper, we use observational data and numerical modeling to present a new explanation for the formation of river-dominated delta networks. Observational data from deltas throughout the world show that distributary channel widths, depths, and lengths decrease nonlinearly with successive bifurcations. Trends in width and depth are an outcome of hydraulic geometry scaling. The trend in channel length is a consequence of delta growth. Analyses of serial maps show that the positions of bifurcations are the fossilized locations of river mouth bars (also called middle-ground and distributary mouth bar) in front of old delta channel mouths. Therefore the trend in channel length can be explained through the mechanics of river mouth bar formation and evolution. We use Delft3D, a coupled hydrodynamic and morphodynamic model, to simulate the process of river mouth bar formation within an expanding turbulent jet in front of distributary channel mouths. Our results describe in detail the formation and evolution of a river mouth bar system and demonstrate that the distance to the river mouth bar is proportional to jet momentum flux and inversely proportional to grain size. Therefore channel length decreases down delta because with each successive bifurcation, the jet momentum flux decreases. These results can be used to predict the future evolution of river-dominated deltas and can be used to aid in hydrocarbon exploration of these depositional environments.

Citation: Edmonds, D. A., and R. L. Slingerland (2007), Mechanics of river mouth bar formation: Implications for the morphodynamics of delta distributary networks, *J. Geophys. Res.*, *112*, F02034, doi:10.1029/2006JF000574.

1. Introduction

[2] What processes form modern delta distributary networks and their orderly topological properties? The distributary network of the Mossy delta, Saskatchewan, Canada, for example (Figure 1), consists of a succession of bifurcations in which the channel widths and lengths to the next bifurcation systematically decrease. While the width trend will be shown to be an outcome of hydraulic geometry scaling relationships, the decrease in distributary channel lengths is not as easily explained. In this paper we seek to understand the origin of these and other topological trends of delta networks by focusing on the processes that give rise to them. Such a detailed study will aid in predicting future behavior of these depositional environments and, from an engineering standpoint, will help improve floodplain and delta management. Also, an understanding of the morphodynamics of river-dominated deltas will lead to better stratigraphic models that more accurately predict the evolution and form of these alluvial sand bodies.

[3] Early work on the topology of delta networks focused on channel vertices and links, allowing *Smart and Moruzzi* [1972] for example, to conclude that the frequency of channel link types can be explained by a model of random connections of vertices. *Morisawa* [1985] then extended this analysis to 20 deltas and found that the frequencies of channel junctions, forks, and links of natural deltas are not random. *Coleman and Wright* [1971] and *Wright et al.* [1974] used field observations and maps to analyze 34 major river systems. Cluster analyses revealed that distributary network patterns are highly variable and cannot be predicted from a single controlling variable. *Mukerji* [1976] analyzed five inland alluvial fans in India and found that the fan network has a consistent shape which is a function of the bifurcation angle at the head of the fan. A global analysis of the world's deltas [*Syvitski et al.*, 2005] revealed that the number of distributary channels within a network is a negative function of delta gradient and a positive function of river length. *Olairu and Bhattacharya* [2006] studied the terminal distributary channels of delta networks and found that within the Volga delta network, channel widths and lengths are log normally distributed, and channel widths decrease exponentially down delta. *Marciano et al.* [2005] showed that tidal channel networks are fractals and channel lengths in a tidal basin decrease by $^1/_2$ with each bifurcation. While *Marciano et al.*'s [2005] result is noteworthy, whether or not it applies to the case of river delta networks remains to be determined. These studies are valuable in quantifying some aspects of delta distributary topology, but they do not address global variation of channel-length scales within a

[1]Department of Geosciences, Pennsylvania State University, University Park, Pennsylvania, USA.

0148-0227/07/2006JF000574$09.00

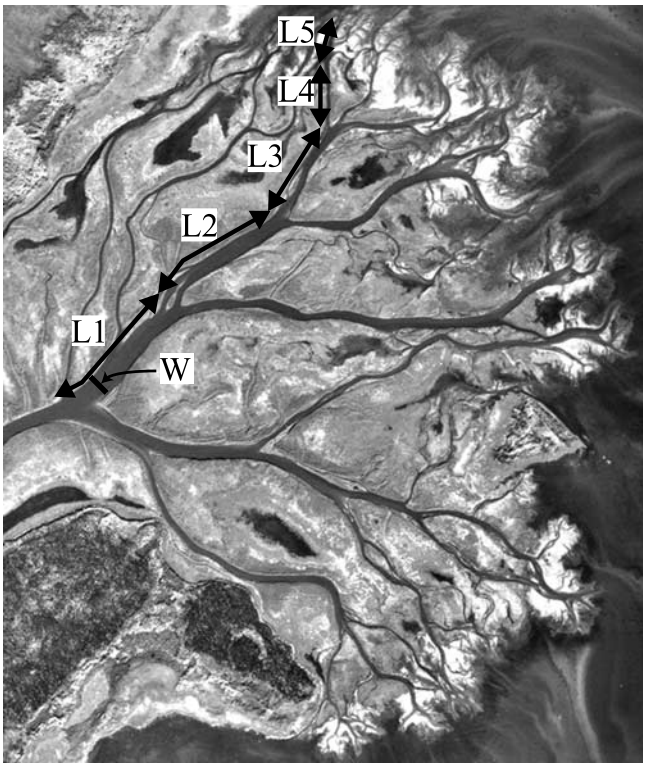

Figure 1. A 1982 aerial photograph of Mossy delta, Saskatchewan, Canada [*Information Service Corporation*, 1982]. The bifurcation length (L) and width (W) decrease with each successive bifurcation of the main channel.

delta, nor do they provide a morphodynamic model that explains the topologic relationships.

[4] The purpose of this paper is to present additional topologic and morphologic data on delta networks and show that these data can be explained using a physically based numerical model of channel elongation and bifurcation around river mouth bars.

2. Observations of Modern Delta Distributary Networks

[5] Topological data were extracted from eleven of the world's deltas. Deltas were selected to minimize the complicating effects of tides and waves [*Wright and Coleman*, 1973; *Wright*, 1977] and to include a broad range of climates, sediment and vegetation types, and river discharges (Figure 2). Topological variables of the deltas were measured on 30-m resolution Landsat 5 images from NASA, aerial photographs, and published maps. On the Landsat images, the 30-m resolution precluded measuring channels narrower than 100 m. Only purely distributary channels—channels that do not rejoin downstream—are included in this analysis. This was done to easily assess how different variables change through multiple bifurcations down the delta. In addition to the planform data, we acquired bathymetric data for Wax Lake, Atchafalaya, and Laitaure deltas.

[6] To characterize the bifurcation geometry and network topology of each delta three variables were measured using GIS software:

[7] 1. Bifurcation length (L) is the distance between two bifurcation points along the channel centerline. A bifurcation point is defined as the upstream intersection of bifurcate channel centerlines. Nondimensional bifurcation length is defined as L/W_o, where W_o is the width of the main river channel before it has split once (here called the zeroth-order channel).

[8] 2. Bifurcation width (W) is the across-stream distance from water edge to water edge on the day the data were recorded. The widths reported are the average of ten measurements from every bifurcation length. Nondimensional bifurcation width is defined as W/W_o.

[9] 3. Bifurcate width (depth) ratio of the wider (deeper) bifurcate arm to the narrower (shallower) arm. For the three deltas with depth data a bifurcation depth (D) was measured. It is defined as the average depth of the cross section of a distributary channel. Nondimensional depth is defined as D/D_o, where D_o is the zeroth-order channel depth.

2.1. Results

[10] To examine how these variables are partitioned within deltas, the data were binned and averaged according to bifurcation order. Bifurcation order is defined as the number of bifurcations upstream of the channel in question. Therefore higher bifurcation orders represent distributary channels farther down the delta.

[11] Nondimensional channel width, channel depth, and channel length averaged across all deltas show well-defined decreases with increasing bifurcation order (Figures 3a, 3b, and 3d). Channel aspect ratio and width ratio (Figures 3c and 3e) are more scattered and, considering the large standard error of the mean, show no definitive trend with bifurcation order.

2.2. Discussion

[12] Standard delta hydraulic geometry relations predict the change in width and depth as discharge decreases with successive bifurcations. If $W = aQ^b$, $D = cQ^k$, and $U = jQ^m$ then from measurements on the bifurcating Laitaure delta, *Andrén* [1994] determined that $a = 9.91$, $b = 0.39$, $c = 0.358$, $k = 0.383$, $j = 0.238$, and $m = 0.227$ whereas on the Volga and Danube delta, *Mikhailov* [1970] found $a = 6.48$, $b = 0.50$, $c = 0.586$, and $k = 0.33$, $j = 0.259$, and $m = 0.167$. Both sets of data can be recast in terms of bifurcation order (n) by assuming that the discharges are split between bifurcate channels in nonlinear proportion to their width. Then the equilibrium width and depth of each channel should decrease in proportion to M^{bn} and M^{kn} respectively, where M is the inverse of the bifurcate width or depth ratio. The resulting curves (solid lines in Figures 3a–3c) are essentially identical to the data measured in this study (Figures 3a and 3b), indicating that average width and depth decrease with increasing bifurcation order because distributary channels are adjusting to a decreasing discharge. Depending on the exponents used [*Andrén*, 1994; *Mikhailov*, 1970] the trend in aspect ratio with bifurcation order should be constant or decreasing (Figure 3c). Although our measured aspect ratios are quite variable, we favor the hydraulic geometry laws of *Andrén* [1994] because channel

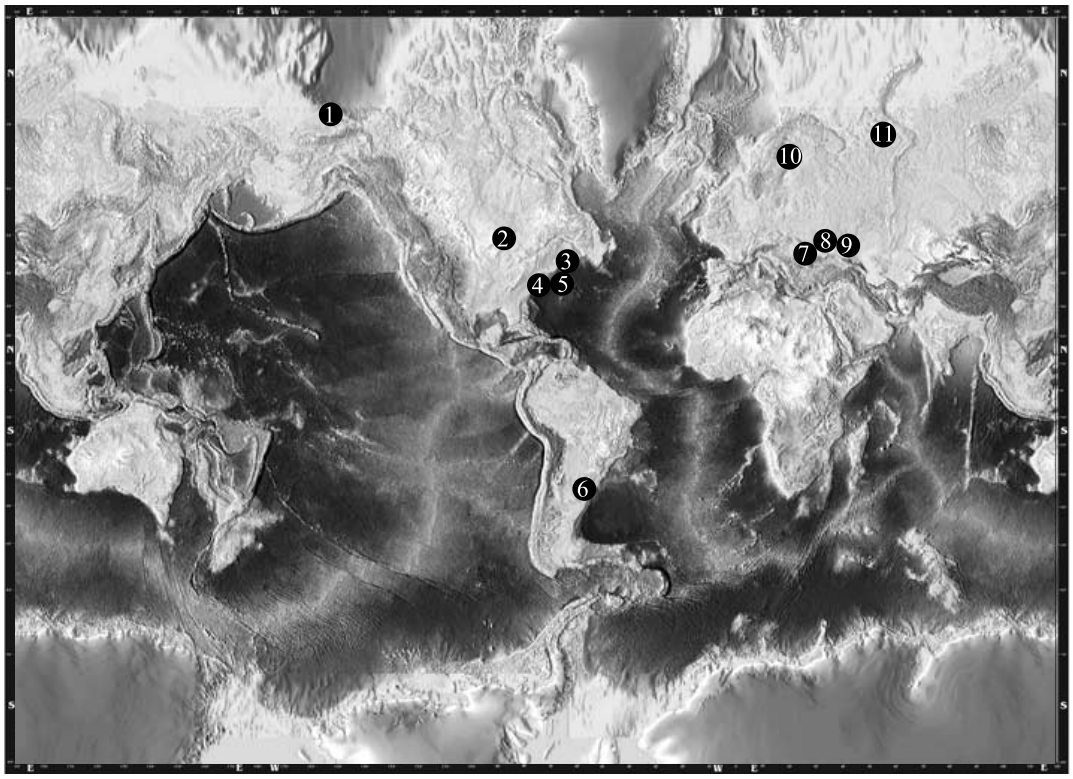

Figure 2. Shaded relief world map showing locations of deltas used in this study. Map is from NOAA 2-min ETOPO2 worldwide digital elevation data.

dredging in lower-order channels of Wax Lake and Atchafalaya delta has artificially decreased their aspect ratios.

[13] There are two observations of distributary channel networks in our study that are not so easily explained. First, as Figure 3d shows, the distance between bifurcations systematically decreases down the distributary networks and the hydraulic geometry laws do not address this. Secondly, the width ratio is invariant up to order five (Figure 3e). Width ratios of the sixth- and seventh-order channels appear to decrease, although the number of cases for which we have data is less than five and therefore the results are probably not meaningful. For bifurcations up to fifth order, the width ratios are not equal but occur most frequently in the ratio of 1.7:1 (Figure 3e). Because this ratio commonly occurs in our data set, it must reflect a morphologically stable configuration at the century timescale. The only theoretical work to address bifurcation stability analysis [*Wang et al.*, 1995; *Bolla Pittaluga et al.*, 2003] found that unequal width ratios are stable, but these authors chose hydraulic and texture parameters of braided streams. Whether these results apply to delta bifurcations is unknown. Intuitively, one might conjecture that a width ratio of 1:1 would be the most stable configuration, making the observed inequality an intriguing result.

[14] In summary, some delta distributary network topology variables exhibit a well defined decrease with bifurcation order. Trends in channel widths, depths, and aspect ratios are consistent with hydraulic geometry scaling. However, trends in channel lengths and width ratios remain enigmatic. To further understand the width and depth trends, and to explain the length trend, we propose the following conceptual model for delta growth.

3. Bifurcation Model for Delta Network Growth

[15] It is understood that the process of bifurcation is a key component in building delta networks [*Bates*, 1953; *Welder*, 1959; *Mikhailov*, 1966; *Axelsson*, 1967; *Baydin*, 1970; *Wright et al.*, 1974; *Wright and Coleman*, 1974; *Wright* 1977; *van Heerden and Roberts*, 1988; *Dumars*, 2002], but we still cannot predict the basic geometries of bifurcations as presented above, nor can we predict the network topology that would arise from a given discharge and sediment caliber. To further our understanding we here develop a general model for delta growth by analyzing the Mossy delta, as captured in four aerial photographs spanning 45 years [*Oosterlaan and Meyers*, 1995]. Subaerial components of the aerial photographs were digitized and analyzed by overlaying each successive delta map.

[16] The digitized maps (Figure 4) suggest that as the delta prograded the network topology was built by two processes: (1) avulsion and (2) channel bifurcation around a river mouth bar. Network generation by avulsion was much less frequent than the process of channel bifurcation around a river mouth bar, and will not be considered further here. Similar serial maps from Atchafalaya delta [*van Heerden and Roberts*, 1988], Wax Lake delta, Cubits Gap splay [*Welder*, 1959], Lake Fausse Pointe delta [*Tye and Coleman*,

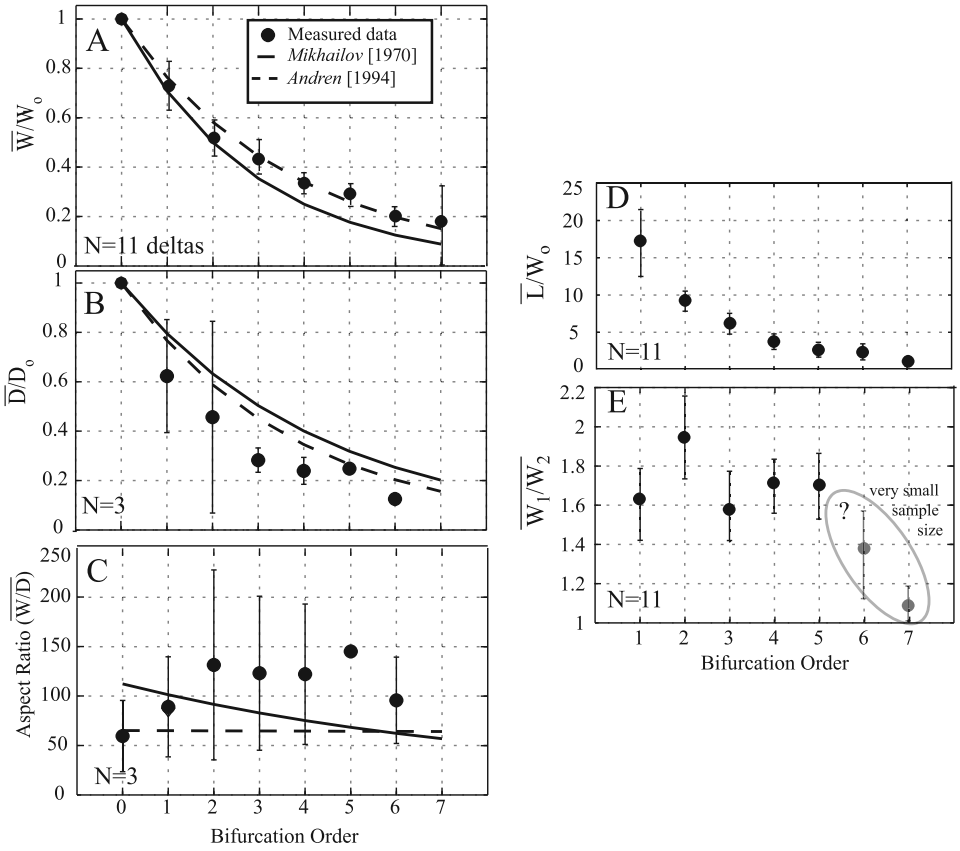

Figure 3. Delta distributary channel geometries as a function of bifurcation order, defined as the number of bifurcations upstream of the channel in question. Data are binned and averaged by bifurcation order. (a) Nondimensional widths for 11 deltas decrease nonlinearly with bifurcation order. Also shown are hydraulic geometry predictions from *Andrén* [1994] and *Mikhailov* [1970] (see text for details). (b) Nondimensional depths for three deltas decrease with bifurcation order, roughly consistent with hydraulic geometry scaling. (c) Aspect ratio shows no definitive trend with order, although hydraulic geometry scaling suggests it should be constant or decreasing. (d) Dimensionless lengths decrease with order. (e) Width ratios show no trend with order. Bars on data points denote standard error of the mean.

1989], Laitaure delta [*Axelsson*, 1967; *Andrén*, 1994], and the Kura River delta [*Mikhailov et al.*, 2003] also confirm the general conclusion that network topology is generated dominantly by bifurcation around a river mouth bar. Therefore, in many deltas, the position of the network bifurcations must be the fossilized locations of river mouth bars that formed in front of old distributary mouths, and the organization and trends within delta networks must be explained through the mechanics of river mouth bar formation.

[17] How do river mouth bars form? It is generally known that at distributary channel mouths sediment-laden flows debouch into a standing body of water in the form of a turbulent plane jet (see review by *Wright* [1977]). The turbulent plane jet at the river mouth experiences lateral and bed friction causing it to decelerate and expand rapidly. The transport capacity of the turbulent jet decreases and sediment is sometimes deposited as a broad radial river mouth bar basinward of the distributary mouth.

[18] Attempts to fill in conceptual detail and quantify these ideas started with *Bates* [1953], who stated that homopycnal or hypopycnal flows lead to river mouth bar development. Bar-forming flows were later reclassified by *Wright* [1977] on the basis of observations of modern systems. He argued that friction-dominated flows, rather than inertial or buoyant flows, entering into shallow bodies of water will likely lead to river mouth bar formation. Of particular interest to this study is the distance to the river mouth bar. Using basic jet theory, *Bates* [1953] conjectured that the river mouth bar will likely form four channel widths basinward of the river mouth because jet centerline velocities begin to decrease there because of jet spreading. This conjecture was contradicted by *Wright and Coleman* [1971] who collected field measurements from ten river-dominated deltas and found that the average distance to the river mouth bars is 10 channel widths, but it should also be noted that the distance from a channel mouth to its mouth bar decreases with increasing channel aspect ratio [*Mikhailov*, 1966]. *Axelsson* [1967] observed in the Laitaure delta that other factors, such as river mouth geometry, grain size, wave influence, and water level variations also significantly influence the depositional pattern of the river mouth bar.

[19] Quantitative models of river mouth bar formation started with *Bonham-Carter and Sutherland* [1967], *Waldrop and Farmer* [1973], and *Farmer and Waldrop* [1977] but

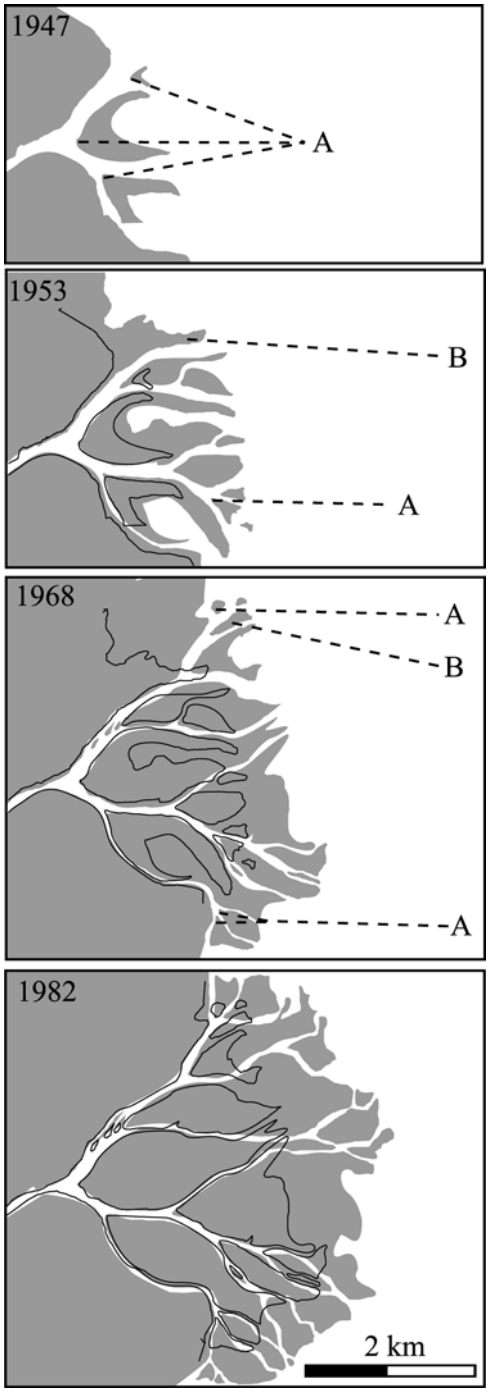

Figure 4. Serial maps of Mossy delta, Saskatchewan, Canada [*Oosterlaan and Meyers*, 1995]. Solid black lines indicate the position of the delta from previous time step. Future bifurcations are formed by two processes: channel splitting around river mouth bars (A) and channel avulsions (B).

these models were two-dimensional, did not simulate turbulence, and did not provide a very satisfying process-based explanation. In an improvement, *Wang* [1984, 1985] used a turbulent, two-dimensional plan view, steady, vertically integrated numerical model of a river-bay-delta system to show that the location of the river mouth bar basinward of the outlet is a function of the dominant particle settling velocity. Furthermore, the planform characteristics of the river mouth bar were shown to be a function of channel depth, basin slope, and centerline velocity. Using a 2-D, plan view numerical model of a tidal jet, *Izumi et al.* [1999] added a bedload transport component and demonstrated that effluent dominated by bedload will lead to river mouth bar construction, while effluent dominated by suspended load will lead to levee construction. Additional numerical modeling studies [*Hatanaka et al.*, 1989; *Butakov*, 1999; *Mashriqui*, 2003] also produced river mouth bars but again offered no detailed explanation for their formation and how their evolution will vary as a function of relative sediment and hydrodynamic parameters.

[20] To further complicate matters, field studies and observations using historic maps, aerial photos, and GIS measurements of river mouth bar evolution reveal that bars are not static features, but actively prograde and aggrade through time. *Lindsay et al.* [1984] observed that the river mouth bar off the tip of the South Pass channel in the Mississippi prograded over 1.1 miles and aggraded 1.2 feet/year from 1867 to 1953. They also documented that the bar advanced primarily though submarine landslides that are triggered when unstable sediment deposited on the bar fails. *Fan et al.* [2006] observed that a river mouth bar offshore of the Huanghe River from 1976 to 1996 prograded 10 to 15 km basinward. These authors concluded that bar formation is dominated by fluvial processes and, in particular, water runoff and variable sediment discharge play an important role in river mouth bar evolution.

[21] *van Heerden and Roberts* [1988] analyzed the formation of a distributary delta using aerial photographs and GIS images. They described two distinct phases of delta growth during the initiation and development of Atchafalaya delta from 1950 to 1982. Rapid deposition immediately basinward of a channel mouth led to channel extension by levee progradation, formation of a river mouth bar, and then rapid bifurcation of the main channel as the wings of the river mouth bar are channelized. Then, as these channels became stabilized and the locus of bifurcation along both bifurcate channels moved basinward, the river mouth bars began to accrete upstream and in some cases amalgamated and closed off channels.

[22] The studies described above provide a conceptual model for river mouth bar formation supported to some extent by field and numerical modeling studies. However, they are still not able to predict the evolution of river mouth bars and their ultimate location and shape at the time of network creation. To answer these questions we present a numerical modeling study of the complete time evolution of a basinward extending channel and a river mouth bar as a function of relevant variables. Important questions to be answered are (1) what hydraulic and sedimentologic conditions are necessary and sufficient for river mouth bar formation; (2) under what hydraulic and sedimentologic conditions do river mouth bars prograde and aggrade; and (3) what process-related variables set the distance to the river mouth bar? Answering these questions will be valuable beyond the immediate application to distributary channel topology. River mouth bars are important hydrocarbon reservoirs [*Flint et al.*, 1988; *Tye et al.*, 1999; *Tye and Hickey*, 2001], and have been widely interpreted in the geologic record [*Hyne et al.*, 1979; *Pulham*, 1989; *Bhattacharya*

and Willis, 2001; *Tye*, 2004; *Turner and Tester*, 2006]. Predicting their formation, evolution, and variation could provide data on their shape, sizes, and spacing that would be useful for reservoir prediction.

4. Numerical Model Description and Setup

4.1. Model Description

[23] We model the processes of river mouth bar formation in an expanding turbulent jet using the computational fluid dynamics package Delft3D [*Lesser et al.*, 2004]. Delft3D simulates fluid flow, waves, sediment transport, and morphological changes at timescales from seconds to years. The equations of fluid, and sediment transport and deposition are discretized on a 3D curvilinear finite difference grid and solved by an alternating direction implicit scheme. An advantage of Delft3D is that the hydrodynamic and morphodynamic modules are fully coupled; the flow field adjusts in real time as the bed topography changes.

4.2. Governing Equations

4.2.1. Conservation of Momentum

[24] Delft3D solves the three-dimensional conservation of momentum equations for unsteady, incompressible, turbulent flow. The *x*-, *y*-, and *z*-directed equations in Cartesian coordinates are

$$\left(\frac{\partial U_x}{\partial t}+U_x\frac{\partial U_x}{\partial x}+U_y\frac{\partial U_x}{\partial y}+U_z\frac{\partial U_x}{\partial z}\right)-fU_y = -\frac{1}{\rho}\left[\frac{\partial p}{\partial x}+\left(\frac{\partial \tau_{xx}}{\partial x}+\frac{\partial \tau_{yx}}{\partial y}+\frac{\partial \tau_{zx}}{\partial z}\right)\right]+g_x \quad (1)$$

$$\left(\frac{\partial U_y}{\partial t}+U_x\frac{\partial U_y}{\partial x}+U_y\frac{\partial U_y}{\partial y}+U_z\frac{\partial U_y}{\partial z}\right)+fU_x = -\frac{1}{\rho}\left[\frac{\partial p}{\partial y}+\left(\frac{\partial \tau_{xy}}{\partial x}+\frac{\partial \tau_{yy}}{\partial y}+\frac{\partial \tau_{zy}}{\partial z}\right)\right]+g_y \quad (2)$$

$$\left(\frac{\partial U_z}{\partial t}+U_x\frac{\partial U_z}{\partial x}+U_y\frac{\partial U_z}{\partial y}+U_z\frac{\partial U_z}{\partial z}\right) = -\frac{1}{\rho}\left[\frac{\partial p}{\partial y}+\left(\frac{\partial \tau_{xz}}{\partial x}+\frac{\partial \tau_{yz}}{\partial y}+\frac{\partial \tau_{zz}}{\partial z}\right)\right]+g_z \quad (3)$$

where U_x, U_y, U_z are the time-averaged *x*-, *y*-, and *z*-directed fluid velocities (m/s); p, f, ρ, τ_{xx}, g are fluid pressure (N/m^2), Coriolis parameter (1/s), density (kg/m^3), fluid shear stress (N/m^2), and acceleration due to gravity (m/s^2), respectively.

4.2.2. Turbulence Closure

[25] There are four different turbulence closure models available in Delft3D to relate the fluid shear stress to the flow velocities. In the course of this investigation, the various closure schemes were compared and the morphologic evolution showed no sensitivity to choice of closure scheme. Therefore the standard $\kappa-\varepsilon$ closure model is used.

4.2.3. Conservation of Fluid Mass

[26] The mass balance equation is given as

$$\frac{\partial U_x}{\partial x}+\frac{\partial U_y}{\partial y}+\frac{\partial U_z}{\partial z}=0 \quad (4)$$

4.2.4. Bedload Transport

[27] The bedload transport formulation per unit width (S_b) employed by Delft3D is from *van Rijn* [1984] and computes the total bedload as estimated by the median diameter:

$$S_b = 0.053\sqrt{(s-1)\cdot g\cdot D_{50}^3}D_*^{-0.3}T^{2.1} \text{ for } T<3.0 \quad (5a)$$

$$S_b = 0.1\sqrt{(s-1)\cdot g\cdot D_{50}^3}D_*^{-0.3}T^{1.5} \text{ for } T\geq 3.0 \quad (5b)$$

where s is the specific density (ρ_s/ρ) and D_{50} is the median particle diameter (m). D_* is the dimensionless particle parameter

$$D_* = D_{50}\left[\frac{(s-1)g}{\nu^2}\right]^{\frac{1}{3}} \quad (5c)$$

where ν is kinematic viscosity (m^2/s). T is the dimensionless transport parameter

$$T=\frac{\left(U_*'\right)^2-\left(U_{*cr}\right)^2}{\left(U_{*cr}\right)^2} \quad (5d)$$

where U_{*cr} is the critical shear velocity (m/s) of the median grain size and

$$U_*'=\left(\frac{C}{C'}\right)^2 U_* \quad (5e)$$

is the effective shear velocity where C is the overall Chezy coefficient and C' is the Chezy coefficient related to grains.

4.2.5. Suspended Transport

[28] The suspended load transport is calculated by solving the three-dimensional diffusion-advection equation

$$\frac{\partial c^i}{\partial t}+\frac{\partial U_x c^i}{\partial x}+\frac{\partial U_y c^i}{\partial y}+\frac{\partial\left(w-w_s^i\right)c^i}{\partial z} = \frac{\partial}{\partial x}\left(\varepsilon_{s,x}^i\frac{\partial c^i}{\partial x}\right)+\frac{\partial}{\partial y}\left(\varepsilon_{s,y}^i\frac{\partial c^i}{\partial y}\right)+\frac{\partial}{\partial z}\left(\varepsilon_{s,z}^i\frac{\partial c^i}{\partial z}\right) \quad (6)$$

where c^i is the mass concentration of the ith sediment fraction (kg/m^3), and w_s^i is the hindered sediment settling velocity of the ith sediment fraction (m/s). $\varepsilon_{s,x}^i$, $\varepsilon_{s,y}^i$, $\varepsilon_{s,z}^i$ are the sediment eddy diffusivities of the ith sediment fraction (m^2/s) in the horizontal (x, y) and vertical (z). The sediment eddy diffusivities are a function of the fluid eddy diffusivities calculated in the equations for fluid flow using horizontal large eddy simulation and grain settling velocity. Delft3D effectively captures the spatial variation in horizontal eddy diffusivity known to exist in diffluences and confluences, as for example in confluences of the Rio Parana River, Argentina (D. Parsons, personal communication, 2006).

4.2.6. Effect of Bed Slope on Sediment Transport

[29] Delft3D accounts for both longitudinal and transverse bed slopes in its sediment transport formulae. The longitudinal flux is increased or decreased for favorable and

Table 1. Description of Different Numerical Grids Used in This Study

Grid	Channel Aspect Ratio	Grid Length, m	Grid Width, m	Centerline Cell Size (L × W), m	Number of Cells (L × W × D)
1	30	2,100	900	30 × 15	70 × 46 × 7
2	60	4,250	1,800	60 × 30	70 × 46 × 7
3	100	7,000	3,000	100 × 50	70 × 46 × 7
4	150	10,500	4,500	150 × 75	70 × 46 × 7
5	300	21,000	9,000	300 × 150	70 × 46 × 7

adverse slopes according to *Bagnold* [1966]. The transverse flux is adjusted according to *Ikeda* [1982].

4.2.7. Changes in Bed Bathymetry

[30] Changes in bed bathymetry are computed from the gradients in sediment transport vectors:

$$\left(1-\varepsilon_{por}\right)\frac{\partial z_b}{dt} = -\frac{\partial S_x}{dx} - \frac{\partial S_y}{dy} + T_d \tag{7}$$

where ε_{por} is the bed porosity, z_b is the bed level (positive up) (m), S_x, S_y are the total sediment transport components per unit width in the x and y directions (m^2/s), and T_d is the deposition or erosion rate of suspended sediment (m/s). For a detailed discussion on the mathematics of Delft3D and the flow/bathymetry interactions see *Lesser et al.* [2004].

4.3. Model Grid Considerations

[31] Delft3D uses a staggered grid where depth points are computed in the center and velocity points and water level points are computed at the midpoint of grid cell edges and grid cell corners, respectively. For our experiments, five separate model grids were used (Table 1). The size of the model grid is scaled to the width of the incoming channel to eliminate grid differences among the runs. The model domain is rectangular with rectangular grid cells whose long axis is parallel to flow. The highest density of grid cells is along the channel centerline.

[32] The numerical experiments in this study were computed in 3D to capture important secondary circulation associated with flow detachment over and around a river mouth bar. In the vertical, there are seven grid cells whose size decreases toward the channel bottom to sufficiently resolve the logarithmic velocity profile. Numerical results should be independent of grid size [*Hardy et al.*, 2003]. We tested for grid independence and found that the gross morphology and evolution of a river mouth bar system were insensitive to our choice of grid size. Therefore we chose a grid that is numerically efficient yet still resolves bathymetric details in the evolving system. All time steps in our experiments obey the Courant-Frederichs-Levy criterion, and therefore the smallest cell in each grid determines the size of the maximum time step.

4.4. Model Setup and Boundary and Initial Conditions

[33] The model is designed to imitate the hydrodynamic and sedimentologic conditions of a river debouching into a still body of water devoid of waves, tides, and positive buoyancy forces, as for example the Mossy River entering Cumberland Lake. The complicating effect of waves and tides cannot be a necessary cause of network regularity because many bifurcating deltas develop on protected coasts that have low tide and wave climates (e.g., Parana, Don, Dnepr, Mossy, Wax Lake, and Atchafalaya). Also, because river mouth bars and channel bifurcations form in freshwater as well as saltwater positive buoyancy forces are ignored. Negative buoyancy forces induced by a heavily sediment-laden flow are accounted for in Delft3D.

[34] The model domain is a rectangle with four open boundaries. A fluvial channel with a temporally and spatially invariant discharge and sediment concentration enters in the middle of the left (west) border. The sediment consists of a single grain size, the caliber of which is varied in the different runs. At the start of each run there is a spatially and temporally constant equilibrium sediment transport rate at the channel inlet.

[35] The three outlet boundary conditions on the north, east, and south boundary consist of temporally and spatially constant water surface elevations. Every numerical experiment was computed for 24 model hours before allowing morphological change. This was done to insure that the initial conditions did not influence the solution and that the appropriate water surface slope and velocity field were developed.

[36] The initial conditions for each numerical experiment consist of an initial bathymetry and an initial 10 m of erodable sediment everywhere in the basin. The grain size of this sediment is equal to the size of the incoming sediment at the inlet. Along the western border a subaerial, sandy shoreline extends one channel width into the reservoir. A trapezoidal channel extending eastward to the open basin is notched within the shoreline. Sensitivity tests show that river mouth bar evolution does not depend on the length of the channelized flow. Basinward of the notched channel is a linearly sloping bed representative of continental shelf slopes around the world.

[37] Delft3D has been validated for a wide range of hydrodynamic, sediment transport, and scour and deposition problems in rivers, estuaries, and tidal basins [*Hibma et al.*, 2004; *Lesser et al.*, 2004; *van Maren*, 2005; *Marciano et al.*, 2005]. However, to assure that the model setup accurately predicts the hydrodynamics of expanding turbulent jets we compared the calculated centerline velocity for a turbulent expanding jet to the theoretical [*Nemec*, 1995] and found that Delft3D is consistent with momentum theory in that the centerline velocity decays as $1/x_c^{1/2}$ within 95% confidence, where x_c is the distance down the centerline of the jet.

4.5. Parameter Space

[38] Consideration of variables in the problem indicates that the depositional pattern in an expanding turbulent jet should be a function of the following dimensional variables: (1) offshore basin slope (J), (2) initial channel width (W) (m), (3) initial channel depth (D) (m), (4) initial channel velocity (U) (m/s), (5) grain size (D_{50}) (m), and (6) gravity

Table 2. Boundary and Initial Conditions for the 55 Numerical Experiments in This Study[a]

RUNID[a]	Width, m	Depth, m	Velocity, m s^{-1}	D50, μm	Slope (10^{-4}), J	Distance to River Mouth Bar, m
121	90	3	1	64	2.5/25	766/796
122	90	3	1	200	2.5/25	646/690
123	90	3	1	1000	2.5/25	406/400
131	90	3	2.7	64	2.5/25	1186/1156
132	90	3	2.7	200	2.5/25	976/946
133	90	3	2.7	1000	2.5/25	660/690
221	180	3	1	64	2.5	840
222	180	3	1	200	2.5	700
223	180	3	1	1000	2.5	570
231	180	3	2.7	64	2.5	1351
232	180	3	2.7	200	2.5	1080
233	180	3	2.7	1000	2.5	790
321	300	3	1	64	2.5/25	1200/1351
322	300	3	1	200	2.5/25	800/900
323	300	3	1	1000	2.5/25	651/600
331	300	3	2.7	64	2.5/25	1600/2151
332	300	3	2.7	200	2.5/25	1451/1500
333	300	3	2.7	1000	2.5/25	1000/1200
421	450	3	1	64	2.5	1300
422	450	3	1	200	2.5	900
423	450	3	1	1000	2.5	800
431	450	3	2.7	64	2.5	1726
432	450	3	2.7	200	2.5	1600
433	450	3	2.7	1000	2.5	1100
521	900	3	1	64	2.5/25	1500/4400
522	900	3	1	200	2.5/25	1200/4200
523	900	3	1	1000	2.5	900
531	900	3	2.7	64	2.5/25	2175/2851
532	900	3	2.7	200	2.5	1551
533	900	3	2.7	1000	2.5	1400
110	90	1.5	1	200	2.5	420
310	300	5	1	200	2.5	1100
510	900	15	1	200	2.5	3000
120	90	1.5	0.75	200	2.5	330
320	300	5	1	200	2.5	1900
520	900	15	2.5	200	2.5	7500
530	1200	20	1.9	200	2.5	9000
200	167	5.7	1.47	200	2.5	1290
300	300	10	2	200	2.5	5000
400	510	16	2.75	200	2.5	7000

[a]The first number of the RUNID corresponds to grid number in Table 1.

(g) (m^2/s). These variables can be assembled into four nondimensional parameters: aspect ratio, W/D, channel Froude number, $U/\sqrt{gD}$, channel grain Froude number, $U/\sqrt{gD_{50}}$, and offshore slope, J. In our experiments, channel aspect ratio varies from 30 to 300, channel Froude number varies from 0.05 to 0.5, and channel grain Froude number varies from 5 to 50. These variations are consistent with measured values on Mossy, Wax Lake, Laitaure, and Atchafalaya delta. Offshore basin slopes of 0.00025 and 0.0025 were used in each run because they are representative of continental shelf slopes around the world [*Kennett*, 1981]. River mouth bars are typically composed of sand-sized sediment [*Dumars*, 2002; *Fielding et al.*, 2005; *Olairu and Bhattacharya*, 2006; *Turner and Tester*, 2006]; therefore, in our experiments, grain size varies from very fine sand (64 μm) to very coarse sand (1000 μm). These different values of variables were combined to produce 55 different model runs. The combinations of variables used in each model are given in Table 2.

4.6. Morphological Scale Factor

[39] To insure that river mouth bars have completely evolved, all numerical results presented hereafter were computed for a period of 750 to 1500 days. A user-defined morphological scale factor is a way to decrease the simulation time of model runs. This is simply an integer multiplying the mass deposition or erosion rate in each time step. A series of sensitivity experiments showed that the final solution is independent of the morphological scale factor if it is less than 200. We used a factor of 75.

5. Results and Discussion of Numerical Modeling

5.1. Spatial and Temporal Evolution of a Subaqueous River Mouth Bar and Levee System

[40] In general, the river mouth bars created in this study initially form basinward of the channel mouth (Figure 5a), prograde basinward (Figure 5b), and then finally stop prograding and begin to widen (Figure 5c). For example, after 25 days of bankfull discharge in RUNID (Figure 5a), the channel has adjusted to the incoming discharge and sediment load by narrowing and scouring a hole extending out to the subaqueous levee tips. Parallel subaqueous levees have developed coincident with the channel wall and extended basinward to approximately $x/W = 3$, where x is distance basinward and W is initial channel width. The levees are in line with, and parallel to, the channel walls

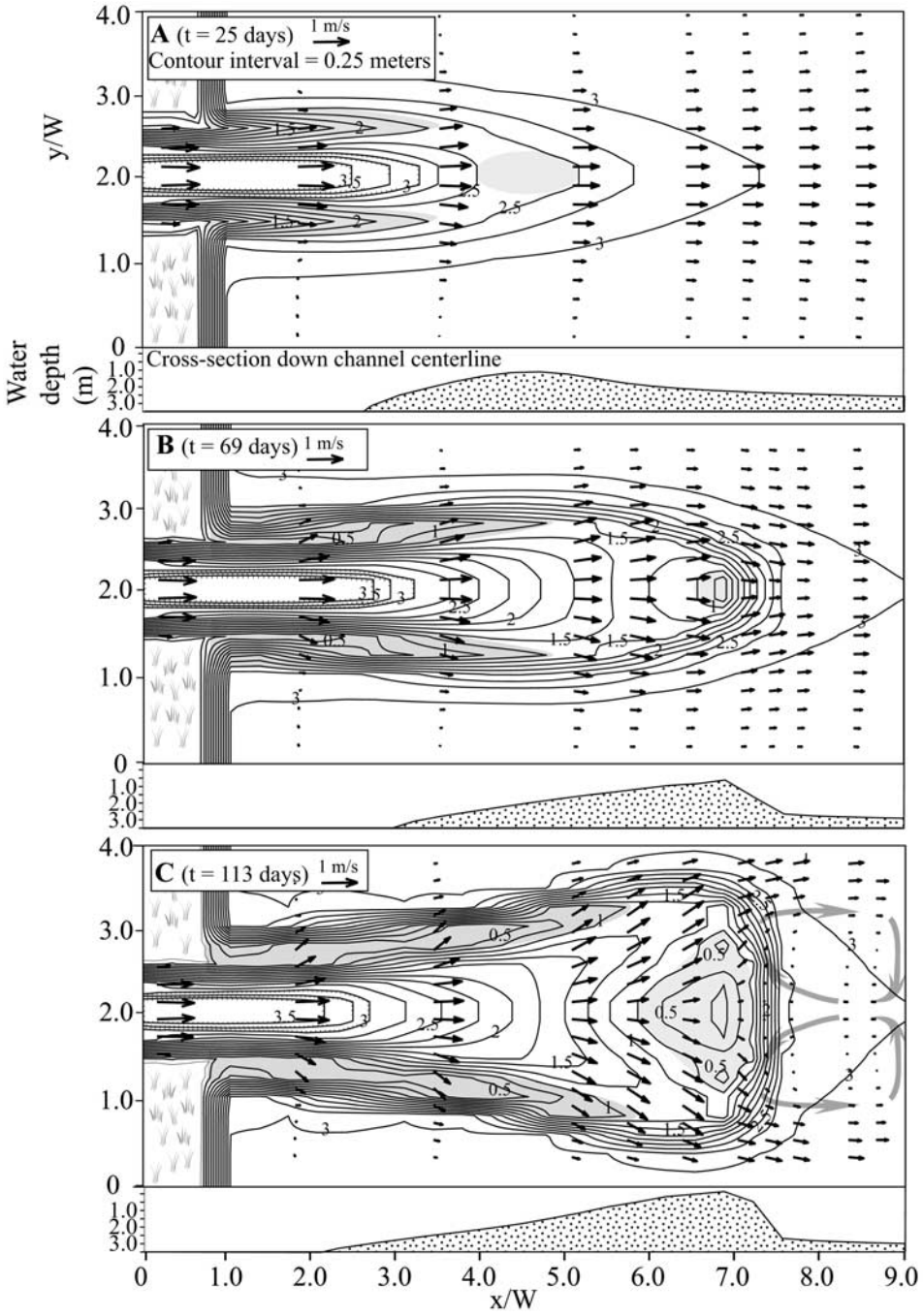

Figure 5. Serial bathymetric contour maps and velocity magnitude vectors depicting the general evolution of river mouth bar system as predicted by Delft3D (RUNID = 122). (a) River mouth bar progrades to $x/W = 5$. (b) Levees continue to grow basinward, but the river mouth bar stops prograding. (c) Levees begin to spread because of the presence of the river mouth bar. The river mouth bar aggrades vertically and widens.

because they are composed primarily of grains transported near the bed. Grain tracking reveals that grains closest to the bed are less likely to be transported significant lateral distances by turbulent eddy advection because they travel lower in the flow column. Basinward of the levee tips along the jet centerline at approximately $x/W = 4.5$ a small river mouth bar is already present, although it produces no noticeable effect on the depth-averaged velocity field. A cross section down the centerline of the jet shows that the river mouth bar has a very gentle front and back slope (cross section in Figure 5a).

[41] After 69 days (Figure 5b), levees have grown laterally and vertically, and extended basinward to approximately $x/W = 4.5$. However, the scour hole remains in the same position. The entire river mouth bar and subaqueous levee system now sits on a raised sediment platform with steep

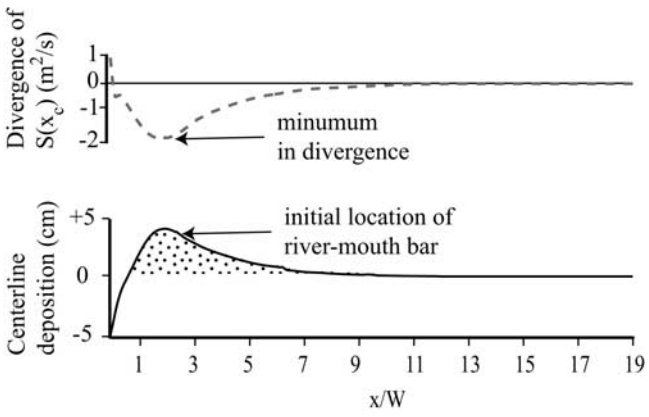

Figure 6. Minimum of the spatial derivative of centerline transport rate ($S(x_c)$) exactly corresponding to the location of the river mouth bar after one time step.

slopes on its downstream and transverse margins. The river mouth bar has prograded basinward to approximately $x/W = 7$ and aggraded enough to produce a low-velocity wake behind the bar. A cross section down the centerline of the jet shows that the slope of the upstream bar face is now shallower, while the slope of bar back has steepened significantly. At this time the bar has stopped prograding.

[42] After 113 days (Figure 5c), the subaqueous levees have extended basinward to approximately $x/W = 6$, and the presence of a large, immobile river mouth bar at $x/W = 7$ has caused the levees to flare. The large river mouth bar has created a back pressure at the upstream face of the bar, leading to sediment deposition and upstream accretion of the bar, as is seen for example on the Atchafalaya delta by *van Heerden and Roberts* [1988]. The entire river mouth bar and subaqueous levee platform has continued to aggrade and the margins have steepened. This aggradation reduces the velocity over the bar top to a fraction of the upstream velocity. Flow separation over the bar top and at bar flanks has created a vigorous recirculation zone in the bar wake (large gray arrows in Figure 5c). Because the bar is static, increased water and sediment discharges around the bar have led to widening and creation of a classic triangular river mouth bar in plan view. Analyses of this and the 55 other simulations allows us to address the following four questions.

5.2. Why Do River Mouth Bars Form?

[43] As a sediment-laden channelized flow at capacity exits into a standing body of water, sediment transport rate (S) down the expanding jet centerline (x_c), decreases basinward because of deceleration of the flow. The flow slows because of its rapid expansion in cross-sectional area during transition from confined to unconfined flow. Along the jet centerline approximately 3% of the total sediment flux is in the cross-stream direction, therefore the sediment transport vector is essentially parallel to the centerline. If the gradient of sediment flux down the centerline ($S(x_c)$) is less than 0, there must be net sediment deposition on the bed. Consequently, the location of maximum sediment deposition should be where the slope of $S(x_c)$ is steepest.

[44] As can be seen in RUNID 122 (Figure 6), before the bar forms the minimum of the divergence of $S(x_c)$ is at $x/W = 1$. After the first time step of sedimentation, the initial location of the bar is coincident with the minimum in divergence. In our runs, the minimum in the divergence of $S(x_c)$ occurs where the jet momentum flux begins to decrease between $0 < x/W < 2$ channel widths into the basin at the point of flow expansion.

[45] Early work claimed that river mouth bar deposition is the result of flow expansion during transition from confined to unconfined flow [*Wright*, 1977]. More specifically we can say that the river mouth bar is created because there is a decrease in jet momentum flux between $0 < x/W < 2$ basinward that creates a high sedimentation rate in this region. Our location of the decrease in jet momentum flux ranges from $0 < x/W < 2$ depending on the initial conditions. This distance is in contrast to *Bates* [1953] who used a simplified momentum theory to conclude that momentum flux begins to decrease four channel widths into the reservoir. Our results are different because we have resolved the process of jet spreading by solving the Reynolds-averaged Navier-Stokes equations.

5.3. Why Do River Mouth Bars Prograde?

[46] After initial formation, river mouth bars prograde because their presence changes the slope of $S(x_c)$ over the bar from negative to positive. This change in slope arises because of flow acceleration on streamlines over the bar. The point of maximum pressure along these streamlines is on the upstream bar face; consequently, fluid velocity is accelerated over the bar leading to erosion of that face and the bar top. With an increase in depth on the back side of the bar, the pressure gradient reverses sign, flow decelerates, and sediment eroded from the upstream bar face is deposited. The net result is bar progradation.

5.4. Why Do River Mouth Bars Stop Prograding?

[47] We conjecture that the river mouth bar stops prograding, or stagnates, when depth over the bar is shallow enough to create a fluid pressure on the upstream side of the bar that is capable of forcing fluid flow around, rather than over, the bar. This leads to deceleration of flow over the bar and runaway aggradation as the shear stress on the bar top falls below critical. To test this conjecture we conducted additional numerical experiments with Delft3D in a rectangular channel with a small, hemispherical river mouth bar in the middle of the grid that was not allowed to erode or grow. The river mouth bar was small enough compared to the grid width and length to eliminate finite grid effects on velocity over the bar. An upstream discharge and a downstream water level boundary condition were used. The water level in the channel was lowered in successive runs so that the depth over the bar (h) became an increasingly smaller percentage of the inlet water depth (h_o).

[48] Modeling results (Figure 7) show that as h/h_o decreases to 0.5, U_{bar}/U_o increases to 1.40, and then with continued shallowing, U_{bar}/U_o becomes much less than one. The h/h_o values when the bars stop prograding in our Delft3D experiments are plotted as a bar graph in Figure 7. Seventy-five percent of the river mouth bars stagnate when the velocity, and therefore the shear stress, rapidly decreases over the bar top at h/h_0 values less than 0.40. At $h/h_0 <$ 0.40, the increased pressure on the upstream side of the bar forces flow around, rather than over the bar, thereby

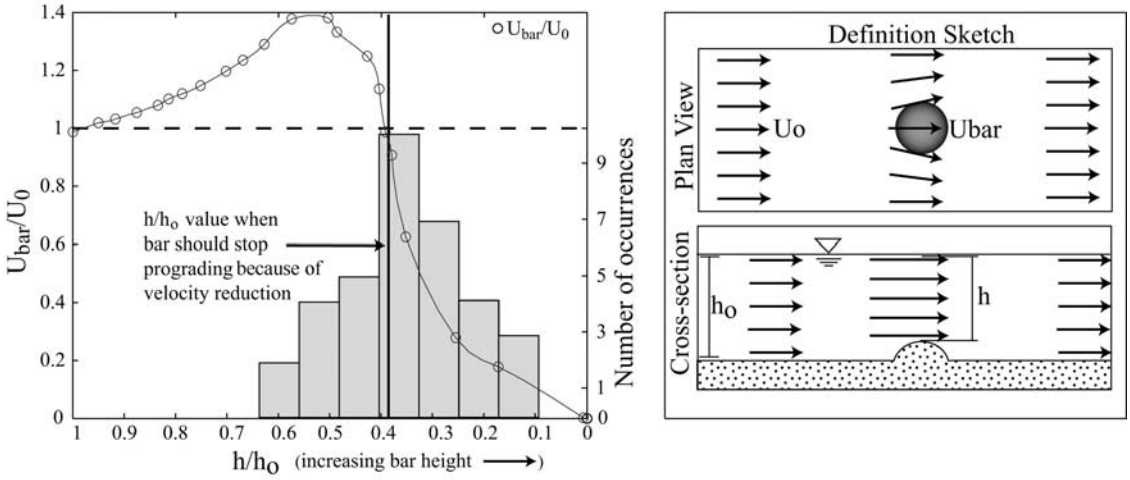

Figure 7. Centerline velocity over a fixed river mouth bar as a function of depth over bar relative to inlet depth. When $1 > h/h_o > 0.5$, velocity increases over the river mouth bar because of flow constriction. When $h/h_o < 0.4$, the velocity decreases over the river mouth bar significantly because increased back pressure at the bar front diverts flow around the bar rather than over. Bar graph shows values of h/h_o when a mobile river mouth bar ceases to prograde in Delft3D experiments. The majority of the bars stagnate after $h/h_o = 0.4$ when velocity over the bar reduces significantly.

decreasing velocity and shear stress over the bar top. This leads to runaway aggradation and the bar stagnates. The distance the bar moves basinward before it stagnates is a function of jet momentum and grain size; the influences of these parameters are discussed in more detail in the following section.

5.5. What Process-Related Parameters Control the Distance to River Mouth Bar?

[49] It is reasonable to assume that the distance to a river mouth bar should be directly proportional to the jet momentum flux and inversely proportional to the grain size. This is born out by our analysis of the model results which suggest that the most important variables influencing distance to river mouth bar (L_{RMB}) are initial channel width (W), initial channel depth (D), initial channel velocity (U), and basin slope (J). These variables can be assembled into three nondimensional parameters, L_{RMB}/D, $\rho WU^2/[(\sigma - \rho)gD_{50}\ W_{max}]$, and J, respectively representing the nondimensional distance to river mouth bar, jet momentum flux relative to unit area grain weight, and basin slope. The modeled nondimensional distance to river mouth bar plotted against momentum flux relative to grain weight (Figure 8) accounts for 87% of the variance of the dependent variable.

[50] The distance to the river mouth bar stagnation point is independent of basin slope (Figure 8). At steeper basin slopes (but where the jet is still attached to the bed) the jet spreading angle decreases. The decreased jet spreading angle is approximately counterbalanced by the increased expansion of the flow in the vertical and thus the rate of change of jet cross-sectional area (A) is the same for the two different slopes. Because the rate of change of A with distance basinward is the same for the different slopes, the centerline velocity profiles (U_c) at different slopes are essentially identical. If A and U_c at any location basinward are the same for different slopes, then the jet momentum flux, ρAU_c^2 in each case is identical. Therefore distance to river mouth bar is invariant with basin slope because that distance is proportional to jet momentum flux (Figure 8) which remains constant for different slopes.

[51] The experimental results reported in Figure 8 were purposefully restricted to cases where positive buoyancy of the jet is unimportant. It is interesting to note however, that four numerical experiments simulating river mouth bar formation in saline water produce the same evolution as described in sections 5.1 to 5.4. These few experiments suggest freshwater-saltwater interactions have little noticeable effect on the distance to the river mouth bar.

[52] The linear regression (Figure 8) can be recast into a power law equation

$$\frac{L_{RMB}}{D} = 104\left[\frac{\rho WU^2}{(\sigma - \rho)gD_{50}W_{max}}\right]^{0.2278} \tag{8}$$

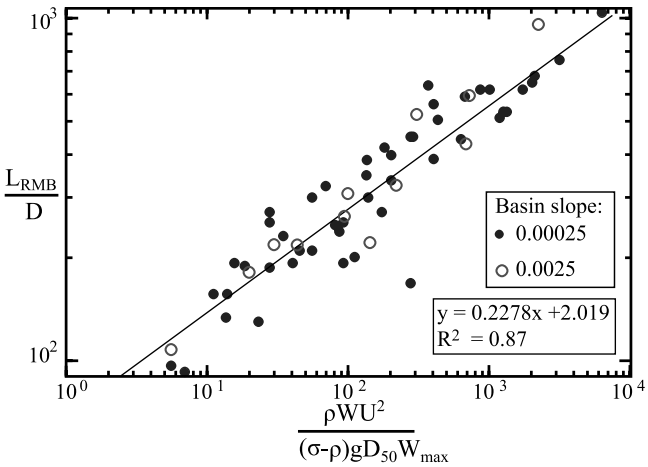

Figure 8. Nondimensional distance to river mouth bar, L_{RMB}/D, increases proportional to jet momentum flux per-unit depth and increases inversely proportional to unit area grain weight.

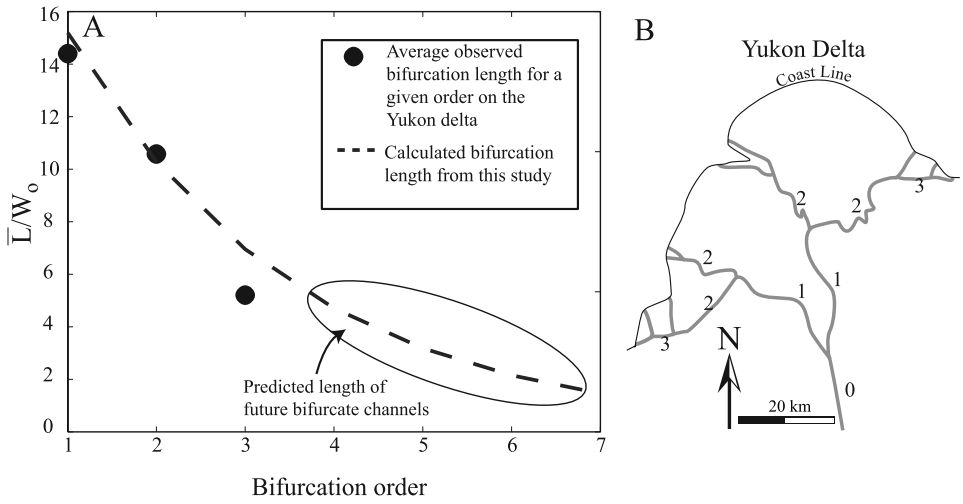

Figure 9. (a) Average length of bifurcate channels for a given bifurcation order in the Yukon delta predicted using equation (10). (b) Map of distributary channels of the Yukon delta. Number on each channel refers to bifurcation order. Only those channels which terminate at a bifurcation were measured.

where W_{max} is the width of the widest channel within the experiments. The distance to river mouth bar (L_{RMB}) is proportional to jet momentum flux divided by grain weight to approximately the one-fifth power.

[53] Which variables in equation (8) exert the strongest control on the distance to a stagnant river mouth bar? A multivariate regression of the data set normalized so that the mean and standard deviation of each variable was 0 and 1, respectively, yields

$$L_{RMB} = 1707 + 1501D + 375U + 190W - 165D_{50} \qquad (9)$$

The coefficients on the variables indicate the relative contributions of each variable. Initial channel depth is the most important variable in determining distance to river mouth bar. It is not surprising that depth is the most important variable, because given our results, in deeper channels river mouth bars will potentially prograde further before reaching the stop criterion of $h/h_o < 0.4$. Velocity also exerts significant control on distance to a river mouth bar because higher velocities increase the jet momentum flux and grains are transported further basinward. Channel width exerts lesser control and grain size is inversely proportional, as expected.

[54] Previous work concluded that the distance to river mouth bar stagnation basinward of the channel mouth is a function of simple grain settling [*Bonham-Carter and Sutherland*, 1967; *Wang*, 1985]. This is based on the notion that grains will begin to fall out of suspension immediately upon flow expansion, reaching the bed at a distance DU/w_s, where w_s is the grain settling velocity. While attractive, this notion does not account for bar progradation observed in the field and captured in our model, and therefore does not accurately predict the final distance to river mouth bar. Another intuitive hypothesis is that the distance to river mouth bar stagnation will be the point where the bed shear stress falls below critical in an expanding turbulent jet. In the experiments reported here that point ranges from x/W = 2.2 to 25 for low and high Froude numbers, respectively. This criterion is not a good prediction of distance to river mouth bar because we find that the stagnation distances in our simulations range from x/W = 3.5 to 12 (Table 2).

[55] While these earlier notions are attractive, they do not account for the complexity of river mouth bar progradation observed in nature. Our work shows that a river mouth bar progrades until the depth over the bar is 40% of the inlet depth and the actual length the river mouth bar progrades is directly and strongly a function of the turbulent jet momentum flux, inversely but weakly a function of grain size, and invariant across a narrow range of basin slopes.

5.6. Application

[56] As an example application of these results we forecast the future evolution of distributary channels in the Yukon delta, Alaska, United States (a delta not in the observational data set of this study). Assuming discharge is split equally at each bifurcation, equation (8) can be rearranged as

$$L_{RMB} = 104\left(\frac{D_0}{2^{Kn}}\right)\left[\frac{\rho}{(\sigma-\rho)gD_{50}}\frac{W_0}{2^{bn}}\frac{U_0^2}{2^{2mn}}\frac{1}{W_{\max}}\right]^{0.2278} \qquad (10)$$

where D_0, W_0, U_0 are the depth, width, and velocity of the zeroth-order bifurcation, n is bifurcation order, and b, K, and m are the exponents from hydraulic geometry relationships. Equation (10) predicts the locations of river mouth bars in front of the channel mouths and consequently predicts the decrease in channel lengths with increasing bifurcation order (Figure 9).

[57] In the field of petroleum geology it is difficult to generate maps of ancient multichannel networks that accurately depict the geometries of deltaic channels (for detailed discussion, see *Olairu and Bhattacharya* [2006]). If the paleodischarge of the delta system can be constrained, the hydraulic geometry relationships and equation (10) can be used to produce a synthetic delta for populating reservoir simulations with realistic sandbody geometries and pore characteristics.

6. Conclusions

[58] There is a class of river-dominated deltas whose networks are formed predominantly by bifurcation around a river mouth bar. These delta distributary networks world-

wide exhibit a systematic decrease in channel lengths, widths, and depths with increasing bifurcation order. Here we have argued from a morphodynamic modeling study that these trends can be explained by the mechanics of river mouth bar formation. There are four stages in the formation of a river mouth bar: (1) as a turbulent jet expands into a shallow, sloping basin it first forms parallel subaqueous levees that extend basinward and then forms a small river mouth bar just basinward of the levee tips; (2) the subaqueous levees extend basinward and the river mouth bar progrades and aggrades; (3) river mouth bar progradation stops and the subaqueous levees continue extending and flare basinward around the stagnant river mouth bar; and (4) finally, the river mouth bar widens and creates the classic triangular river mouth bar in plan view.

[59] River mouth bars form because the cross-sectional area of the expanding jet increases and consequently the sediment transport rate down the jet centerline decreases basinward as flow progresses from confined to unconfined. The minimum in the divergence of the centerline transport flux at the transition point precisely defines the initial location of the river mouth bar. River mouth bars then prograde because their presence causes flow acceleration on streamlines over the bar. This acceleration changes the sediment transport gradient over the bar from negative to positive causing net erosion on the upstream bar face and net deposition in the downstream bar wake. River mouth bars stop prograding when the depth over the bar is equal to or less than 40% of the inlet depth because fluid pressure on the upstream side of the bar is large enough to divert flow around the bar. The distance to a final river mouth bar stagnation location in front of the distributary channel tip is a positive function jet momentum flux and inversely proportional to unit area grain weight. Multivariate regression reveals that depth and velocity exert the strongest controls on the location of river mouth bar stagnation.

[60] These results help explain the network topology relationships of delta distributary channels. Channels within distributary networks follow hydraulic geometry relationships, and therefore as discharge decreases with every bifurcation the widths and depths decrease as M^{qn}, where q is the appropriate hydraulic geometry exponent. Downstream of a newly formed bifurcation, the channel depth is shallower and available time for river mouth bar progradation decreases because the vertical aggradation distance required to meet the stop criterion of $h/h_o < 0.4$ decreases. Furthermore, the discharge and velocity are decreased thereby decreasing the momentum and the average grain transport distance basinward. Thus the distance to the next bifurcation decreases with bifurcation order because depth and velocity decrease with each bifurcation. Future work includes quantifying how temporally variant water discharge, waves, Coriolis acceleration, and positive buoyancy affect the geomorphic evolution of deltas.

Notation

C Chezy coefficient, nondimensional;
C' Chezy grain coefficient, nondimensional;
c^i concentration in the flow of the ith sediment fraction, kg m^{-3};
D channel depth, m;
D_* van Rijn particle parameter, nondimensional;
D_0 channel depth of zeroth bifurcation order, m;
D_{50} median grain size, m;
f Coriolis parameter, s^{-1};
g acceleration due to gravity, m s^{-2};
h depth above river mouth bar, m;
h_0 channel depth at inlet boundary, m;
J offshore bed slope, nondimensional;
L bifurcation length, m;
L_{RMB} distance to river mouth bar, m;
M inverse of width or depth ratio of bifurcate channels;
n bifurcation order, nondimensional;
p pressure, N m^{-2}
Q water discharge, m^3 s^{-1};
s specific density, nondimensional;
$S(x_c)$ magnitude of total sediment transport rate down jet centerline, m^2 s^{-1};
S_b magnitude of bedload transport, m^2 s^{-1};
$S_{x,y}$ total sediment transport in x or y dimension, m^2 s^{-1};
t time, s;
T sediment transport parameter, nondimensional;
T_d deposition or erosion rate of suspended sediment, m s^{-1};
U velocity magnitude, m s^{-1};
U_* shear velocity, m s^{-1};
U'_* effective shear velocity, m s^{-1};
$U_{*,cr}$ critical shear velocity, m s^{-1};
U_{bar} velocity over the river mouth bar, m s^{-1};
U_o velocity of zeroth order bifurcation, m s^{-1};
$U_{x,y,z}$ velocity components, m s^{-1};
W bifurcation width, m;
W_0 width of zeroth bifurcation order, m;
x,y,z planform (x, y) and vertical dimension (z), m;
z_b bed level, m;
$\varepsilon^i_{x,y,z}$ sediment eddy diffusivity of the ith sediment fraction, m^2 s^{-1};
ε_{por} bed porosity, nondimensional;
ν kinematic viscosity, m^2 s^{-1};
ρ fluid density, kg m^{-3};
σ density of quartz, kg m^{-3};
τ_{ij} i-directed momentum from j-directed fluid shear stress, N m^{-2};
w^i_s hindered settling velocity of the ith sediment fraction, m s^{-1}.

[61] **Acknowledgments.** This research was done while D.A.E. was supported by NSF grant EAR-0417877 awarded to R.L.S. D.A.E would like to thank Scott Miller and Evan Goldstein for many useful discussions regarding earlier versions of this manuscript. The authors would like to thank David Hoyal for useful discussions about delta dynamics and river mouth bars. We are grateful to two anonymous reviewers whose insightful comments strengthened this manuscript.

References

Andrén, H. (1994), Development of the Laitaure delta, Swedish Lapland: A study of growth, distributary forms, and processes, Ph.D. thesis, 188 pp., Inst. of Earth Sci. Phys. Geogr., Uppsala Univ., Uppsala, Sweden.

Axelsson, V. (1967), The Laitaure delta: A study of deltaic morphology and processes, *Geogr. Ann., Ser. A, Phys. Geogr.*, *49*, 1–127.

Bagnold, R. A. (1966), An approach to the sediment transport problem from general physics, *U.S. Geol. Surv. Prof. Pap.*, *422-1*, 37 pp.

Bates, C. C. (1953), Rational theory of delta formation, *AAPG Bull.*, *37*, 2119–2162.

Baydin, S. S. (1970), Formation of modern delta branches on non-tidal rivers with large sediment discharge, in *Hydrology of Deltas*, vol. 1,

Proceedings of the Bucharest Symposium, May, pp. 113–120, Int. Assoc. of Hydrol. Sci., Vienna.
Bhattacharya, J. P., and B. J. Willis (2001), Lowstand deltas in the frontier formation, Powder River basin, Wyoming: Implications for sequence stratigraphic models, *AAPG Bull.*, *85*, 261–294.
Bolla Pittaluga, M., R. Repetto, and M. Tubino (2003), Channel bifurcations in braided rivers: Equilibrium configurations and stability, *Water Resour. Res.*, *39*(3), 1046, doi:10.1029/2001WR001112.
Bonham-Carter, G. F., and A. J. Sutherland (1967), Diffusion and settling of sediments at river mouths: A computer simulation model, *Trans. Gulf Coast Assoc. Geol. Soc.*, *17*, 326–338.
Butakov, A. N. (1999), A one-dimensional mathematical model of a river mouth bar, *Water Resour.*, *26*, 22–28.
Coleman, J. M., and L. D. Wright (1971), Analysis of major river systems and their deltas: Procedures and rationale with two examples, *Tech. Rep. 95*, 100 pp., Coastal Stud. Inst., La. State Univ., Baton Rouge.
Dumars, A. J. (2002), Distributary mouth bar formation and channel bifurcation in the Wax Lake delta, Atchafalaya Bay, Louisiana, M. S. thesis, 88 pp., La. State Univ., Baton Rouge.
Fan, H., H. Huang, T. Q. Zeng, and K. Wang (2006), River mouth bar formation, riverbed aggradation and channel migration in the modern Huanghe (Yellow) River delta, China, *Geomorphology*, *74*, 124–136.
Farmer, R. C., and W. R. Waldrop (1977), A model for sediment transport and delta formation, *Waterw. Port Coastal Ocean Div. Am. Soc. Civ. Eng.*, *5*, 102–115.
Fielding, C. R., J. D. Trueman, and J. Alexander (2005), Sharp-based, flood-dominated mouth bar sands from the Burdekin River delta of northeastern Australia: Extending the spectrum of mouth-bar facies, geometry, and stacking patterns, *J. Sediment. Res.*, *75*, 55–66.
Flint, S., D. J. Stewart, T. Hyde, E. C. A. Gevers, O. R. F. Dubrule, and E. D. Van Riessen (1988), Aspects of reservoir geology and production behavior of Sirikit oil field, Thailand: An integrated study using well and 3-D seismic data, *AAPG Bull.*, *72*, 1254–1269.
Hardy, R., S. Lane, S. Ferguson, and D. Parsons (2003), Assessing the credibility of a series of computational fluid dynamic simulations of open channel flow, *Hydrol. Processes*, *17*, 1539–1560.
Hatanaka, K., M. Kawahara, and S. S. Y. Wang (1989), A finite element application of sand terrace formation process, paper presented at the International Symposium of Sediment Transport, Am. Soc. of Civ. Eng., New York.
Hibma, A., H. Schuttelaars, and H. J. De Vriend (2004), Initial formation and long-term evolution of channel-shoal patterns, *Cont. Shelf Res.*, *24*, 1637–1650.
Hyne, N. J., W. A. Cooper, and P. A. Dickey (1979), Stratigraphy of intermontane, lacustrine delta, Catatumbo river, Lake Maracaibo, Venezuela, *AAPG Bull.*, *61*, 2042–2057.
Ikeda, S. (1982), Lateral bed load transport on side slopes, *J. Hydraul. Div. Am. Soc. Civ. Eng.*, *108*, 1369–1373.
Information Service Corporation (1982), Aerial potograph of Mossy Delta in Lake Cumberland, *Photo CSMA-90482-15-L6B 70*, Regina, Sask., Canada.
Izumi, N., H. Tanaka, and M. Date (1999), Inceptive topography of fluvial-dominated river mouth bars, in *Proceedings of the Seventh International Symposium on River Sedimentation*, edited by A. W. Jayawardena, J. H. W. Lee, Z. Y. Wang, and A. A. Balkema, Brookfield, Vt.
Kennett, J. (1981), *Marine Geology*, Prentice-Hall, Upper Saddle River, N. J.
Lesser, G., J. Roelvink, J. Van Kester, and G. Stelling (2004), Development and validation of a three-dimensional morphological model, *Coastal Eng.*, *51*, 883–915.
Lindsay, J. F., D. B. Prior, and J. M. Coleman (1984), Distributary-mouth bar development and role of submarine landslides in delta growth, South Pass, Mississippi delta, *AAPG Bull.*, *68*, 1732–1743.
Marciano, R., Z. B. Wang, A. Hibma, H. J. De Vriend, and A. Defina (2005), Modeling channel patterns in short tidal basins, *J. Geophys. Res.*, *110*, F01001, doi:10.1029/2003JF000092.
Mashriqui, H. S. (2003), Hydrodynamic and sediment transport modeling of deltaic sediment processes, Ph.D. thesis, 146 pp., Civ. and Environ. Eng., La. State Univ., Baton Rouge.
Mikhailov, V. N. (1966), Hydrology and formation of river mouth bars, in *Problems of the Humid Tropical Zone Deltas*, vol. 1, *Proceedings of the Dacca Symposium*, pp. 59–64, U. N. Educ., Sci. and Cult. Organ., Paris.
Mikhailov, V. N. (1970), Hydrologic-morphometric characteristics of delta branches, *Stud. Rep. Hydrol.*, *9*, 146–158.
Mikhailov, V. N., V. I. Kravtsova, and D. V. Magritskii (2003), Hydrological and morphological processes in the Kura River delta, *Water Resour.*, *30*, 495–508.
Morisawa, M. (1985), Topologic properties of delta distributary networks, in *Models in Geomorphology*, edited by M. J. Woldenberg, pp. 239–268, Allen and Unwin, St Leonards, NSW, Australia.
Mukerji, A. B. (1976), Terminal fans of inland streams in Sutlej-Yamuna plain, India, *Z. Geomorphol.*, *190*, 190–204.
Nemec, W. (1995), The dynamics of deltaic suspension plumes, in *Geology of Deltas*, edited by M. N. Oti and G. Postma, pp. 31–93, Balkema, A. A. Brookfield, Vt.
Olairu, C., and J. P. Bhattacharya (2006), Terminal distributary channels and delta front architecture of river-dominated delta systems, *J. Sediment. Res.*, *76*, 212–233.
Oosterlaan, S., and M. Meyers (1995), Evolution of the mossy delta in the relation in hydrodam construction and lake level fluctuation, undergraduate thesis, 29 pp., Univ. of Ill., Chicago.
Pulham, A. J. (1989), Controls on internal structure and architecture of sandstone bodies within upper carboniferous fluvial-dominated deltas, county Clare, western Ireland, *Spec. Publ. Geol. Soc. London*, *41*, 179–203.
Smart, J. S., and V. L. Moruzzi (1972), Quantitative properties of delta channel networks, *Z. Geomorphol.*, *16*, 283–300.
Syvitski, J. P. M., A. J. Kettner, A. Correggiari, and B. W. Nelson (2005), Distributary channels and their impact on sediment dispersal, *Mar. Geol.*, *222–223*, 75–94.
Turner, B. R., and G. N. Tester (2006), The table rocks sandstone: A fluvial, friction-dominated lobate mouth bar sandbody in the Westphalian B coal measures, NE England, *Sediment. Geol.*, *190*, 97–119.
Tye, R. S. (2004), Geomorphology: An approach to determining subsurface reservoir dimensions, *AAPG Bull.*, *88*, 1123–1147.
Tye, R. S., and J. M. Coleman (1989), Evolution of Atchafalaya lacustrine deltas, south-central Louisiana, *Sediment. Geol.*, *65*, 95–112.
Tye, R. S., and J. J. Hickey (2001), Permeability characterization of distributary mouth bar sandstones in Prudhoe Bay field, Alaska: How horizontal cores reduce risk in developing deltaic reservoirs, *AAPG Bull.*, *85*, 459–475.
Tye, R. S., J. P. Bhattacharya, J. A. Lorsong, S. T. Sindelar, D. G. Knock, D. D. Puls, and R. A. Levinson (1999), Geology and stratigraphy of fluvio-deltaic deposits in the Ivishak formation: Applications for development of Prudhoe Bay field, Alaska, *AAPG Bull.*, *83*, 1588–1623.
van Heerden, I. L., and H. H. Roberts (1988), Facies development of Atchafalaya delta, Louisiana: A modern bayhead delta, *AAPG Bull.*, *72*, 439–453.
van Maren, D. S. (2005), Barrier formation on an actively prograding delta system: The Red River delta, Vietnam, *Mar. Geol.*, *224*, 123–143.
van Rijn, L. C. (1984), Sediment transport; part I, Bed load transport, *J. Hydraul. Eng.*, *110*, 1431–1456.
Waldrop, W. R., and R. C. Farmer (1973), Three-dimensional flow and sediment transport at river-mouths, technical report, 137 pp., Coastal Stud. Inst., La. State Univ., Baton Rouge.
Wang, F. C. (1984), The dynamics of a river-bay-delta system, *J. Geophys. Res.*, *89*, 8054–8060.
Wang, F. C. (1985), The Atchafalaya river delta: Analytical analysis of the development of the Atchafalaya river delta, *Tech. Rep. HL-82-15*, 199 pp., U.S. Army Eng. Waterw. Exp. Stat., Vicksburg, Miss.
Wang, Z. B., M. Devries, R. J. Fokkink, and A. Langerak (1995), Stability of river bifurcations in 1D morphodynamic models, *J. Hydraul. Res.*, *33*, 739–750.
Welder, F. A. (1959), Processes of deltaic sedimentation the lower Mississippi river, *Tech. Rep. 12*, 90 pp., Coastal Stud. Inst., La. State Univ., Baton Rouge.
Wright, L. D. (1977), Sediment transport and deposition at river mouths: A synthesis, *Geol. Soc. Am. Bull.*, *88*, 857–868.
Wright, L. D., and J. M. Coleman (1971), Effluent expansion and interfacial mixing in the presence of a salt wedge, Mississippi river delta, *J. Geophys. Res.*, *76*, 8649–8661.
Wright, L. D., and J. M. Coleman (1973), Variations in morphology of major river deltas as functions of ocean wave and river discharge regimes, *AAPG Bull.*, *57*, 370–398.
Wright, L. D., and J. M. Coleman (1974), Mississippi river mouth processes: Effluent dynamics and morphologic development, *J. Geol.*, *82*, 751–778.
Wright, L. D., J. M. Coleman, and M. W. Erickson (1974), Analysis of major river systems and their deltas: Morphologic and process comparisons, technical report, 114 pp., Coastal Stud. Inst., La. State Univ., Baton Rouge.

D. A. Edmonds and R. L. Slingerland, Department of Geosciences, Pennsylvania State University, University Park, PA 16802, USA. (dedmonds@geosc.psu.edu)